Evaluation of WRF Parameterizations for Climate Studies over Southern Spain Using a Multistep Regionalization

DANIEL ARGÜESO, JOSÉ M. HIDALGO-MUÑOZ, SONIA R. GÁMIZ-FORTIS, AND MARÍA JESÚS ESTEBAN-PARRA

Departamento de Física Aplicada, Facultad de Ciencias, Universidad de Granada, Granada, Spain

JIMY DUDHIA

National Center for Atmospheric Research, Boulder, Colorado

YOLANDA CASTRO-DÍEZ

Departamento de Física Aplicada, Facultad de Ciencias, Universidad de Granada, Granada, Spain

(Manuscript received 3 February 2011, in final form 15 April 2011)

ABSTRACT

This paper evaluates the Weather Research and Forecasting model (WRF) sensitivity to eight different combinations of cumulus, microphysics, and planetary boundary layer (PBL) parameterization schemes over a topographically complex region in southern Spain (Andalusia) for the period 1990–99. The WRF configuration consisted of a 10-km-resolution domain nested in a coarser domain driven by 40-yr European Centre for Medium-Range Weather Forecasts Re-Analysis (ERA-40) data, with spectral nudging above the PBL employed over the latter domain. The model outputs have been compared at different time scales with an observational dataset that comprises 438 rain gauges and 152 temperature stations with records of both daily maximum and minimum temperatures. To reduce the ''representation error,'' the validation with observations has been performed using a multistep regionalization that distinguishes five precipitation regions and four temperature regions.

The analysis proves that both cumulus and PBL schemes have a crucial impact on the description of precipitation in Andalusia, whereas no noticeable differences between microphysics options were appreciated. Temperature is described similarly by all the configurations, except for the PBL choice affecting minimum values.

WRF provides a definite improvement over ERA-40 in the climate description in terms of frequency, spatial distribution, and intensity of extreme events. It also captures more accurately the annual cycle and reduces the biases and the RMSE for monthly precipitation, whereas only a minor enhancement of these features was obtained for monthly-mean maximum and minimum temperatures. The results indicate that WRF is able to correctly reproduce Andalusian climate and produces useful added-value information for climate studies.

1. Introduction

The climate response to global warming varies from region to region; thus, regional projections of scenarios are essential to determine its repercussions for population and environment, since both are mainly affected by local changes. General circulation models (GCMs) have been extremely useful in providing comprehensive predictions of large-scale climate and general circulation (Gillett and Thompson 2003; Osborn 2004; Solomon et al. 2007); however, they are still unable to resolve local circulation dynamics. The computational costs of increasing spatial resolution in GCMs are still prohibitive and alternative approaches have been promoted, such as regional climate models (RCMs), which enable high-resolution runs over restricted areas (Dickinson et al. 1989; McGregor 1997; Giorgi 2006; Laprise 2008).

Prior to making use of RCMs for high-resolution projections, it is crucial that model estimates be evaluated

Corresponding author address: Daniel Argüeso, Departamento de Física Aplicada, Facultad de Ciencias, Universidad de Granada, Campus de Fuentenueva, s/n C.P. 18071 Granada, Spain.
E-mail: dab@ugr.es

DOI: 10.1175/JCLI-D-11-00073.1

against observational data to assess their reliability in capturing spatial and temporal distributions (Leung et al. 2003; Laprise et al. 2008; Kostopoulou et al. 2009). Despite the importance of model validation, there is no consensus on the evaluation procedure, and methodological improvement remains a major task for climate modelers. Furthermore, the evaluation is still hindered by a number of factors. The increase of RCM resolution is much faster than the development of climate observation networks, and very few regions are covered by a dense enough observational system. A useful approach is that of using observational gridded datasets that facilitate the evaluation (Evans and McCabe 2010). Nevertheless, available gridded analyses, such as the Climatic Research Unit time series 1.2 (CRU TS 1.2) (Mitchell et al. 2004), are sometimes created with very sparse observations in certain areas, such as southern Spain. The lack of both consensual and systematic methodologies and the scant observational data at researchers' disposal has led to several validation strategies.

Traditionally, model results are directly compared with in situ observations, although this is not a like-with-like comparison (Rivington et al. 2008). Site-specific measurements describe conditions at single stations affected by very local characteristics, whereas the RCM outputs define average values of the variables over a grid box. In areas with complex terrain, the ''representation error'' is of particular importance because the station might be at the extreme of the cell topographical diversity. Accordingly, the most appropriate way to validate a model is to use upscaled observations (Göber et al. 2008). Other techniques have been suggested, such as adjusting model outputs, either through a lapse rate depending on elevation differences between the site and the model grid point (Moberg and Jones 2004) or using a downscaling factor calculated from deviations between observational time series and model estimates (Rivington et al. 2007). Although the comparability of these adjusted outputs with observations remains unproven.

To upscale observations, regionalization procedures have been put forward within the framework of RCM evaluation for different variables (Jiménez et al. 2008; Caldwell et al. 2009; Kostopoulou et al. 2009). Some authors have highlighted the convenience of regionalization in terms of model validation because it filters very local station effects that models cannot resolve (Bunkers et al. 1996; Reid and Turner 2001). Original climate divisions (Köppen 1923; Thornthwaite 1931) have the advantage of direct applicability and simplicity, even though they are formulated in a subjective way. To reduce subjectivity several methods have been recently employed to attempt climate regionalization using objective techniques across the globe (Bärring 1987; Fovell 1997; Gerstengarbe et al. 1999; Romero et al. 1999; Unal et al. 2003).

The Weather Research and Forecasting model (WRF; Skamarock et al. 2008) has been used to achieve dynamical downscaling, and this paper presents its evaluation as a nested climate model over Andalusia (southern Spain). Located at the very southern part of Europe (35°–40°N, 8°–1°W), Andalusia is largely influenced by three differentiated masses: the Atlantic Ocean, the Sahara desert, and the Mediterranean Sea (Fig. 1). The Intergovernmental Panel on Climate Change (IPCC) Fourth Assessment Report (AR4) (Solomon et al. 2007) predicts this area to be among those most affected by climate change, with marked precipitation decrease and summer warming. In addition, it is an extremely complex terrain region with mountains exceeding 3000 m within 40 km of the Mediterranean coast, strong surface extremes, arid regions, and very confined climate regimes defined by mesoscale weather systems.

Many of these features occur on spatial scales unresolved by the model, and so require empirical parameterization. A wide range of parameterization schemes is provided by WRF along with other configuration options so, considering the complex region under investigation, optimizing the configuration is a key factor for climate research over this area. Seldom is a configuration optimal for all the locations, for all the variables, and at every time scale (Fernández et al. 2007; Borge et al. 2008); nonetheless, a compromise can be made to adequately describe the climate over the entire region. Beyond the combination of parameterization schemes, other factors should be explored, such as the driving data reliability or the influence of the domain design. Consequently, setting up the model correctly is a challenging task involving many aspects that must be considered.

Several studies have focused on selecting appropriate configurations or particular WRF parameterizations for varying conditions and applications (Jankov et al. 2005; Gallus and Bresch 2006; Kain et al. 2006; Borge et al. 2008; Deb et al. 2008; Hong et al. 2009; Kwun et al. 2009; Li and Pu 2009; Nolan et al. 2009), but because of computational costs, little effort has been devoted to this topic for interannual studies and different physical parameterizations (Bukovsky and Karoly 2009). For climate purposes, longer periods are preferable when identifying configurations that describe as correctly as possible the local climate rather than particular periods. Accordingly, a 10-yr period (1990–99) has been selected in this study to test the model sensitivity for both wet and dry years. Although it also might be argued that longer periods are still convenient to actually represent climate, this 10-yr period permits obtaining robust results that

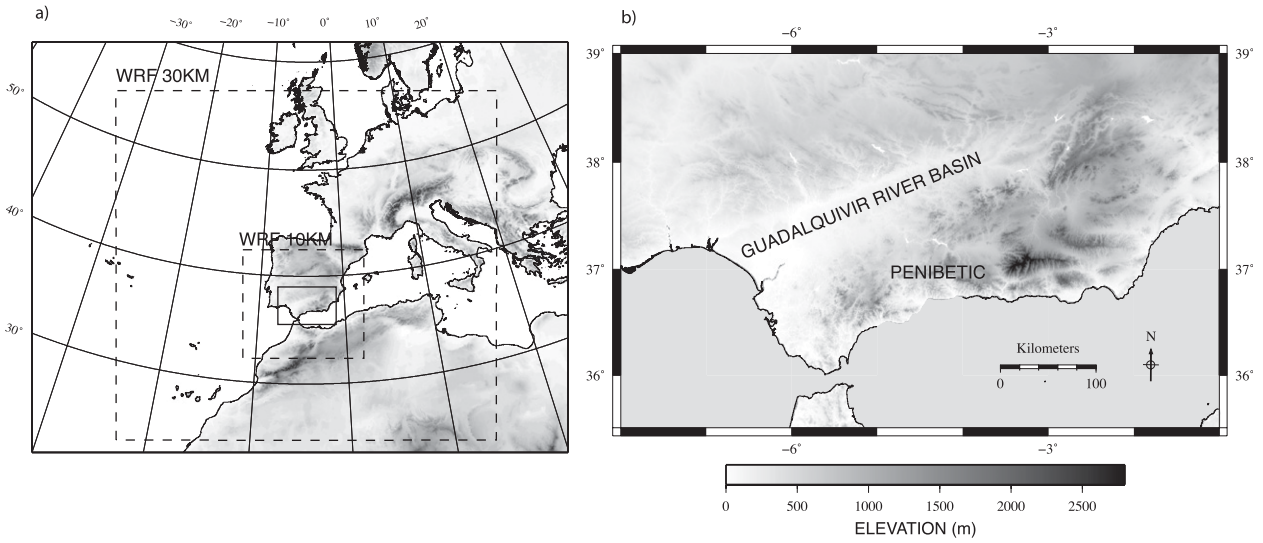

FIG. 1. (a) WRF domains (dotted squares) and resolutions. Region of interest (solid line). (b) Topographical features of southern Spain.

are not restricted to the specific conditions of a particular year.

The outline of the paper is as follows: In section 2, observational and reanalysis data are presented together with the quality controls and the model setup. A multistep regionalization procedure is described in section 3. Reviewing different simulations and their performances over the region, as presented in section 4, helps to evaluate the most appropriate configuration in general terms. The final section summarizes and provides a discussion of the main findings of the study.

2. Model setup and data

a. Model description and configuration

Version 3.1.1 of WRF was used for dynamical downscaling. This model provides many different physical and running options for a wide spectrum of applications at very different scales, from large-eddy simulation (Catalano and Cenedese 2010; Catalano and Moeng 2010) to climate simulations (Sertel et al. 2009; Zhang et al. 2009). Physical options are composed of parameterization schemes to describe subgrid-scale processes, such as cumulus, microphysics, planetary boundary layer (PBL) turbulence, long-wave and short-wave radiation, and land surface models.

Initial and boundary conditions were obtained from the 40-yr European Centre for Medium-Range Weather Forecasts (ECMWF) Re-Analysis (ERA-40). Other reanalysis datasets, such as the National Centers for Environmental Prediction–National Center for Atmospheric Research Reanalysis Project (NNRP), were also evaluated but were discarded because they showed large sea surface temperature (SST) cold biases in the western Mediterranean that induced unacceptable deviations in inland temperatures. A 6-h interval was chosen to update boundary conditions, as suggested by Denis et al. (2003), for an integration with similar spatial resolution. The original T159 spectral resolution, with 11 vertical levels and four soil levels, was interpolated to a 1.125° × 1.125° regular latitude–longitude resolution.

In WRF 3.1, spectral nudging was included to reduce the effects of domain location and geometry and to prevent synoptic-scale climate drift generated by the formulation of lateral boundary conditions over an open system during long-term simulations (Miguez-Macho et al. 2004; Radu et al. 2008). The integration area is known to affect internal variability (Seth and Giorgi 1998; Christensen et al. 2001), and spectral nudging reduces the impact of the domain design but retains large-scale features so that the model domain choice is not that critical.

The spatial setup of WRF was composed of two domains, a 30-km-resolution parent domain with 130 × 120 grid points and a 10-km one-way nested domain with 124 × 112 grid points (Fig. 1). The time steps were recommended for these horizontal resolutions, that is, 180 and 60 s, respectively. Both domains had 35 vertical levels arranged according to terrain-following hydrostatic pressure vertical coordinates. This study focuses on high-resolution integrations, so only the 10-km domain was analyzed. All the WRF simulations were initialized on 1 June 1989 and ended on 31 December 1999. Although previous studies (Giorgi and Mearns 1999; Fernández 2004) proved that initial values have minor effects on results, a 7-month spinup period was used to

TABLE 1. Parameterization combinations to perform the physics ensemble with WRF.

Cumulus	PBL	Microphysics	ID
BMJ	MYJ	WSM-3	BM3
BMJ	MYJ	Thompson et al.	BMT
BMJ	ACM2	WSM-3	BA3
BMJ	ACM2	Thompson et al.	BAT
BMJ	YSU	WSM-3	BY3
BMJ	YSU	Thompson et al.	BYT
KF	MYJ	WSM-3	KM3
KF	MYJ	Thompson et al.	KMT

ensure model equilibrium between external forcing and internal dynamics, especially in terms of soil variables, which normally require longer spinups. Therefore, the period 1990–99 was analyzed.

Eight simulations were run using spectral nudging above the PBL and only over the coarse domain. The spectral nudging employed was reasonably weak, setting the wavenumber to 1 (~3900 km) and the frequency to 24 h. Table 1 details the different schemes that were combined, varying the cumulus [Kain–Fritsch (KF) and Betts–Miller–Janjic (BMJ)], the PBL [Yonsei University (YSU), Mellor–Yamada–Janjic (MYJ), and asymmetric convective model version 2 (ACM2)], and the microphysics [WRF single-moment three-class (WSM-3) and Thompson et al.]. Radiation schemes were set to the Community Atmosphere Model (CAM) for both longwave and shortwave, owing to the fact that it permits modifying greenhouse gas (GHG) concentrations and thus their effect on radiation. Regarding the land surface model (LSM), only the Noah LSM was used because it is widely adopted for climate studies (Sertel et al. 2009; Zhang et al. 2009). Some preliminary tests were performed using Grell 3D cumulus and the five-layer soil model, but these were clearly outperformed by other schemes and thus were discarded at the first stages of the study.

The accuracy of the model configured with a certain scheme cannot be uniquely attributed to a single parameterization but rather to the combination of them, since feedbacks are usually as important as the schemes themselves. Furthermore, the suitability of a specific configuration strongly depends on the region, the season, or even the particular event considered and hence, there is no single configuration appropriate for every situation. Since testing all the possible combinations of physics options is not computationally affordable, a representative sample of the physics packages was chosen with a different level of complexity and formulation.

The original formulation of WRF was modified in the version Climate WRF (clWRF) at the University of Cantabria (Fita et al. 2010), which introduces many additional options. For instance, it permits updating GHG concentrations or computing daily maximum temperature (T_{max}) and minimum temperature (T_{min}) at every time step, making model outputs much more comparable to observational data.

b. Observational data

Model outputs were validated against an observational database retrieved from the regional government of Andalusia (Subsistema de Climatología Ambiental, Consejería de Medio Ambiente, Junta de Andalucía). It consists of homogeneous daily maximum and minimum temperature time series from 152 stations, and daily rainfall series from 438 gauges across Andalusia (Fig. 2), with coverage throughout 1990–99. The period was selected as a compromise between the number of available stations and the maximum possible length to represent climate features. Initially, the available dataset comprised 1821 precipitation series and 850 temperature series that were filtered on the basis of a 10% threshold of missing values for the selected period. Nevertheless, the discarded series have not been completely rejected

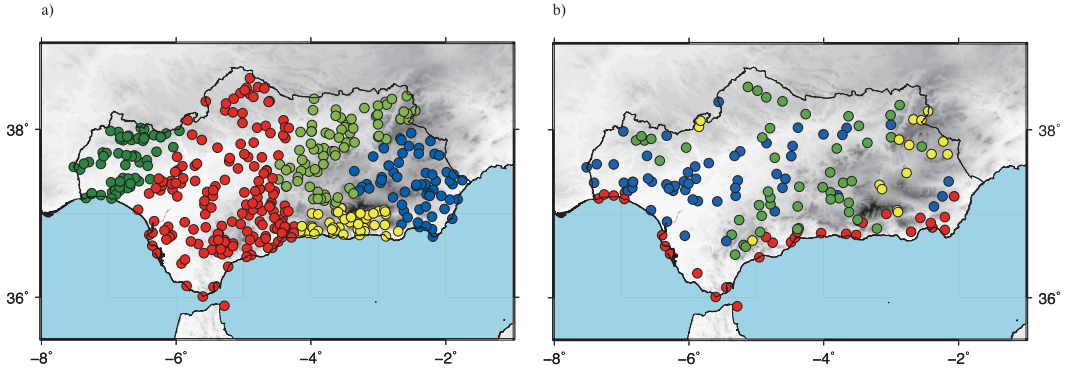

FIG. 2. Regions obtained with the multistep methodology for (a) precipitation: W (dark green), C (red), N (light green), S (yellow), and E (blue); (b) temperature: CO (red), HL (yellow), ML (green), and LL (blue).

and those containing more than 70% coverage have been used to fill the gaps of the final selection using a multiple linear regression method with the five most correlated stations. Completeness of the observational series is required not for direct comparison with model outputs but for the regionalization methodology described in the next section.

3. Regionalization methodology

Clustering analysis (CA; Kalkstein et al. 1987) and principal component analysis (PCA; Preisendorfer 1988) are the most extended methodologies to classify stations into regional divisions (Richman and Lamb 1985; Fovell and Fovell 1993; Lund and Li 2009). Both procedures have advantages and shortcomings in relation to climate regionalization, as shown below for PCA and two different CA algorithms:

1) PCA reduces information redundancy and keeps only the most important variability modes, leading to a more comprehensive division. However, the fuzzy nature of results makes it difficult to determine regional boundaries.
2) Hierarchical or agglomerative CA methods successively merge clusters based on a similarity measure starting from as many single-element clusters as initial objects and finally reaching one cluster, accommodating all the stations. Several solutions varying the number of clusters are proposed and an optimal configuration can be selected through tests that measure the clusters' internal cohesion and external isolation. Nonetheless, the formulation prevents the exchange of objects between clusters once they have been merged and therefore certain objects might be misplaced.
3) Nonhierarchical CA algorithms such as *k*-means require prespecification of the number of clusters and their centroids (seeds) and thus are not suitable for determining an appropriate configuration by themselves. Conversely, they are based on the exchange of objects and enable cluster redistribution.

In this paper, a multistep methodology is proposed, consisting of the consecutive application of PCA and two CA algorithms, overcoming the problems that each method presents. The procedure permits, using the results from each analysis, to carry out the subsequent steps, removing most of the subjectivity associated with researcher's decisions, such as the number of regions or their centroids.

Standardization problems and the rare coincidence of temperature and precipitation records encouraged us to process these variables independently. The approaches to process both temperature and precipitation were very similar, although some minor modifications were introduced in the data preparation (e.g., precipitation was screened) because of obvious differences in the variables' characteristics.

At a first level, the covariance matrix obtained from daily values over the period 1990–99 was analyzed using an S-mode PCA to retain principal modes of variability and discard possible information redundancy (Fovell 1997). The North rule of thumb, based on the eigenvalue degeneration (North et al. 1982), was adopted here and the resulting significant principal components (PCs) were varimax rotated to increase spatial coherence. Rotated normalized loadings were then processed to classify the stations via a two-step CA (Milligan 1980) comprising an agglomerative method to set the number of clusters and their starting seeds, followed by a nonhierarchical *k*-means algorithm. This strategy takes advantage of both methods and reduces their respective imperfections.

Regarding the hierarchical method, the simplest and most extended squared Euclidean distance was chosen to measure the similarity between objects and clusters. According to previous results (Kalkstein et al. 1987; Gong and Richman 1995), the average linkage algorithm was selected to assign objects membership to clusters because it does not tend to create similar-size groups nor huge ''hungry'' clusters as other methods do.

Hierarchical algorithms merge clusters in new ones based on the principle of maximizing intracluster similarity and minimizing intercluster likeness. The ratio between these two values varies as the clusters are merged and tests, such as pseudoF (Calinski and Harabasz 1974), measure it at every step. This way, pseudoF led us to define an optimal number of divisions when a local maximum was attained.

Next, the clusters centroids were calculated using the rotated normalized loadings and fed into a nonhierarchical *k*-means CA along with the suitable number of clusters, so relocation of the stations is performed.

As stated before, $T_{\min}$, $T_{\max}$, and precipitation have very different features and hence separate preprocessing of data is advisable. Further, these three variables will yield two independent regionalizations—one for temperature and one for precipitation—that must be analyzed individually.

a. Regionalization of precipitation

Precipitation in Andalusia is mainly concentrated in short rain events and shows an explicit annual cycle with very dry summers. Therefore, it seems appropriate to apply a filter so that dry days at most of the locations are removed and accurate rainfall regionalization can be

achieved. The approach suggested by Romero et al. (1999) for a similar region was followed, consisting of retaining only those days when the precipitation was larger than 5 mm for at least 5% of the stations, resulting in 654 days over the 10-yr period.

The covariance S-mode PCA computed with this reduced precipitation dataset produced five significant principal modes that in total explained 57.75% of the variance. According to the hierarchical algorithm, the pseudoF indicated that a five-cluster organization is more appropriate for precipitation. Higher numbers of clusters are also suggested by the test (12 and 17), but they over fragmented this small region. After the *k*-means CA, some stations were misplaced and clearly isolated with respect to the surrounding region, so they were relocated on the basis of an inverse distance weighting over the nearest five stations. Only 6 of 438 stations needed such reassignment. Therefore, it is reasonable to assume that the procedure does not noticeably affect the results; however, the spatial coherence of the classification was enhanced.

The final precipitation regionalization is shown in Fig. 2a, generating a coherent structure of climate divisions corresponding to the topography and the main features of the dominating circulation. An evident zonal partitioning can be observed that accounts for the gradual influence of fronts coming from the Atlantic Ocean and systems generated in the Mediterranean Sea. Moreover, topography effects can be seen in the boundaries of regions north (N), south (S), and east (E), delimited by the Sierra Nevada ridge and the Subbetic Mountain system. The eastern precipitation regime is clearly distinguished from the other Andalusian rainfall patterns; indeed, this semiarid-to-arid area, with markedly convective character and differentiated dynamical precipitation, is accurately singled out by the regionalization technique. An almost identical regionalization was obtained in one of the solutions proposed by Romero et al. (1999), with minor differences probably caused by the inclusion of the whole Spanish Mediterranean coast in their study.

b. Regionalization of temperature

Unlike precipitation, temperature was not screened and the full-length series were used to characterize regions. The temperature climate division was performed using both T_{max} and T_{min} because these two variables are not equally affected by the same factors (i.e., stratification versus turbulence, surface fluxes, elevation). For example, the T_{max} at two stations might present a similar evolution and magnitude, but the T_{min} might differ considerably. Therefore, they must be considered separately in the PCA to avoid masking the information provided by one of the temperature extremes by the other.

North's rule of thumb indicated five significant components for T_{max} (94.92% of the total variance explained) and three for T_{min} (91.37% of the total variance explained). The normalized loadings were varimax rotated, merged, and fed into the average linkage clustering based on an 8D distance that includes both T_{max} and T_{min} rotated loadings. The pseudoF test suggested that a four-cluster division is the simplest configuration among those recommended. The *k*-means were calculated afterward using the seeds obtained from the hierarchical CA to permit the exchange of stations between regions. The relative sparseness of the temperature stations in comparison to precipitation leads to more heterogeneous regions, also influenced by the fact that temperature directly hinges on elevation, and hence the regions are considerably scattered. Consequently, the relocation of isolated stations was skipped here since it would substantially reshape the regions because boundaries are not as defined as they were for precipitation.

As shown in Fig. 2b, the coastal (CO) region is distributed along the coast (red); the highlands (HL) region includes stations at high altitudes ranging from 760 to 1350 (yellow); stations located in the lower Guadalquivir River basin and the interior of the eastern part (blue) conform the lowlands (LL); and the midlands (ML) region (green) covers those internal stations that are situated in the mountains but at lower elevations than the highlands.

Summarizing, 438 rain gauges were divided into five regions and 152 temperature stations were classified in four regions. This regionalization was used to validate WRF outputs in a comprehensive way and overcome the issue related to the representation error, as shown in the next section.

4. Model evaluation and sensitivity tests

In this section, different parameters that were calculated to validate the model at varying time scales against the observations, grouped in the regions that were obtained previously for precipitation (five regions) and temperature (four regions), are shown.

A key motivation to use dynamical downscaling is to increase the spatial resolution over a certain area, which should have a noticeable impact on the distribution and magnitude of the extreme events. To evaluate the improvement introduced by WRF in this respect, different percentiles were calculated as a representation of the probability distribution function (PDF) and compared against observations. From a climate point of view, it is interesting to note that WRF reproduces the PDF of daily values rather than the timing of particular events.

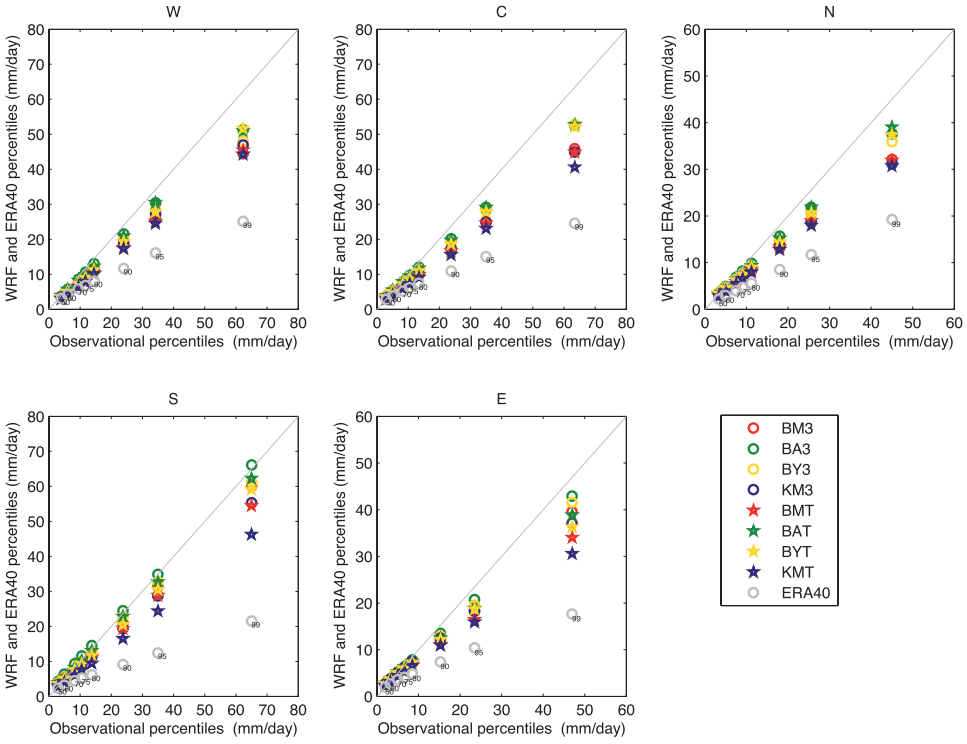

FIG. 3. Daily precipitation percentiles simulated by various WRF configurations and ERA-40 vs observational percentiles for the different regions. Gray line indicates a perfect description of the PDF.

In addition, monthly means were calculated to assess the capability to represent the annual cycle and highlight the seasons when the largest differences between the WRF results and observations occur. Correlation, root-mean-square error (RMSE), and mean absolute error (MAE) were computed to ascertain whether the model is able to capture interannual temperature variability. By contrast, correlation, relative RMSE (RMSE divided by the monthly-mean precipitation), and bias were analyzed for precipitation. Different parameters were calculated for precipitation and temperature in accordance with their different nature. These parameters, along with the percentile values, let us determine the most suitable physics configuration for southern Spain in terms of reproducing climate features for both temperature and precipitation using WRF.

Results are shown within climate zones, and the spatial distribution of those parameters is also presented for the selected configurations with the aim of discovering possible WRF limitations over Andalusia.

a. Precipitation results

1) DAILY VALUES OF PRECIPITATION

The percentiles (50th, 60th, 70th, 75th, 80th, 90th, 95th, and 99th) of daily events were computed, taking into account rainy days defined by a 0.1 mm day^{-1} threshold. Figure 3 shows the percentiles for WRF and observations corresponding to each region. The gray line represents a perfect performance, delimiting over- and underestimation. Percentiles obtained from ERA-40 are also presented.

Throughout the five regions identified, WRF tends to underestimate precipitation extremes, except for the south region, where the combination BA3 (refer to Table 1 for expansions of parameterization combinations) captures remarkably well all the percentiles calculated, with a slight overestimation. Overall, this configuration provides the most accurate results, yielding values within 10% of the magnitude of the observed events for even the most extreme conditions (99th percentile). Some other physics combinations (BY3, BAT, and BYT) perform similarly or even better for particular areas or thresholds. While the cumulus parameterization seems to have a noticeable influence in describing extremes, microphysics appears to have a minor impact on this climate feature, with no regional superiority among the schemes, apart from the south and east areas, where WSM3 produces slightly better results. The south and east regions are located along the Mediterranean coast and therefore more affected by convective precipitation. A correct partition of precipitation into convective and

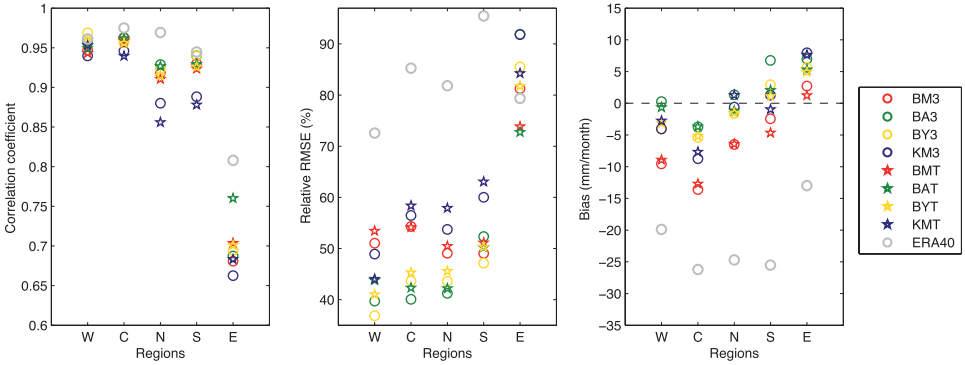

FIG. 4. (left to right) Correlation coefficient, relative RMSE, and bias calculated for WRF and ERA-40 monthly precipitation with respect to observations in the different regions.

nonconvective, as well as an appropriate feedback between cumulus and microphysics, might explain why the south and east extremes are particularly well reproduced. Regarding the PBL schemes, both the ACM2 and the YSU yield similar results, with minimal differences in favor of ACM2.

A clear enhancement in characterizing extremes has already been revealed as one of the main advantages of dynamical downscaling (Frei et al. 2003; Bell et al. 2004; Giorgi 2006), and indeed a notable improvement is achieved with WRF in terms of percentiles. This improvement might be exclusively associated with an increase in the spatial resolution with respect to boundary data. However, the dependence of WRF results upon the different physics configurations suggests that, despite the undeniable effect of resolution, physics must also play an important role in reproducing precipitation extreme events.

2) MONTHLY VALUES PRECIPITATION

Accumulated monthly precipitation was calculated for every station and its nearest WRF grid point, and then spatially averaged to obtain the monthly series for each region. The correlation coefficient, relative RMSE, and bias between WRF and the observational series are shown in Fig. 4. The same procedure was adopted with ERA-40 so that the improvement associated with WRF could be evaluated.

All three parameters values—correlation, RMSE, and bias—are within a satisfactory range, apart from the east region. The correlation coefficients vary from 0.90 and 1.00, excluding the east region (0.65–0.76) and some simulations that employed the Kain–Fritsch cumulus scheme over the north and south regions. Relative RMSE is acceptable for every region, except for the east, where it reaches values as large as 92% of the average monthly precipitation. In contrast, the best combination for each of the other regions never exceeds 50% of the average monthly rainfall. The differences in the monthly-mean precipitation displayed in terms of the bias show a tendency to underestimate total precipitation in the western regions [west (W) and central (C)] and overestimate in the east (east and south regions).

Concerning WRF performance with respect to its boundary conditions, ERA-40 monthly correlations with observations are higher than WRF correlations (except the west region), whereas both the bias and the RMSE are substantially worse. An evident improvement is attained with WRF, reducing by about half the error corresponding to ERA-40 in most of regions. Again, different behavior can be observed in the east region, where although the bias is clearly reduced in absolute value and has opposite sign, RMSE is similar for both model results and reanalysis. This feature, plus the low correlation, indicates that WRF might not be able to capture the timing as it would be desired, but it is able to noticeably refine reanalysis estimations of total precipitation over the east region.

The east region (Mediterranean coast) is widely known for its singularity regarding precipitation, since the marked convective nature of rain in semiarid climates complicates the accurate description of total precipitation amount and location (Amengual et al. 2007). Not only WRF but also ERA-40 shows a pronounced difference in correlation for the east region compared with the other areas, and hence errors might be partly inherited from the boundary conditions. An additional cause for such spatial distribution of correlation and bias is related to large-scale precipitation, and it might be attributed to the smoothing of mountain ridges and weakening of the associated "rain shadow" because of the selected resolution. Most of the fronts that arrive in the Iberian Peninsula come from the

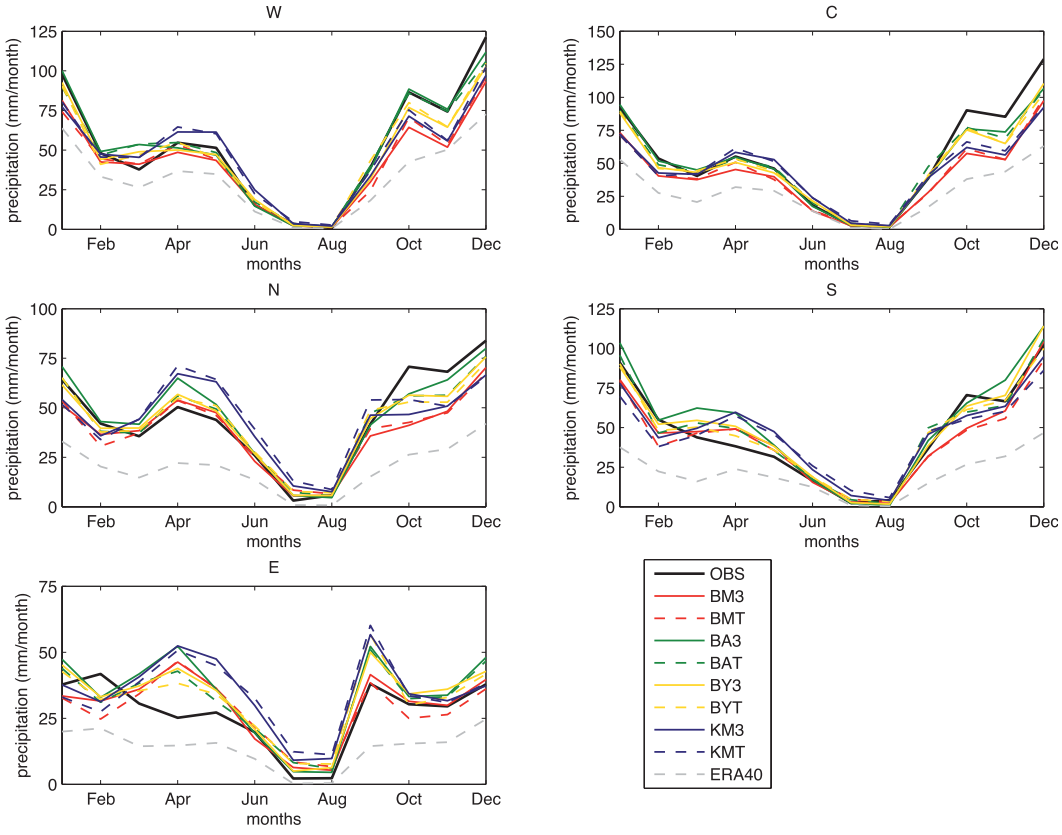

FIG. 5. Annual cycle of monthly precipitation for the different regions: observations (black), ERA-40 data (gray dashed), and WRF simulations (colors).

Atlantic Ocean and the mountains constitute an orographic barrier, creating a semiarid region to their east. The model possibly lets too many fronts into the east region, leading to a positive bias (Fig. 4).

The annual cycle with monthly means was also calculated for the 10-yr study period to identify the WRF performance in different seasons. WRF broadly captures the annual cycle (Fig. 5), including features not represented by boundary conditions. For instance, the local minimum in November is represented by WRF to varying degrees. Andalusian precipitation is characterized by a summer minimum in August with basically no rain events and a maximum during December and January, which are also well reproduced by WRF.

In contrast, spring rainfall seems to be systematically exaggerated by WRF in the north and south regions, whereas autumn precipitation is underestimated in most of the regions. Precipitation in the eastern region is remarkably overestimated, primarily in April, May, and, to a lesser extent, September; the latter can be attributed to an excess of soil moisture due to a positive deviation in August precipitation that might enhance evaporation and thus convective rainfall after summer. In fact, summer deviations in precipitation only take place in the east region. In contrast, spring errors cannot be univocally attributed to a single source and different causes might contribute to these deviations (i.e., a misrepresentation of topography, an enhancement of land surface thermal contrast, or a deficient simulation of Mediterranean cyclogenesis that produces a large fraction of the east coast precipitation). This is not a WRF-exclusive feature but a common deficiency in RCMs over the Iberian Peninsula (Herrera et al. 2010) that would require further investigation.

Although the ERA-40 monthly correlation is high for most of the regions, the annual cycle is too flat and WRF actually provides a sharper depiction of it. This indicates that WRF is introducing interesting details in terms of monthly precipitation for climate studies. The combination using BMJ–ACM2 (BA3 and BAT) appears to be the most accurate in reproducing the annual cycle, especially in the central and west regions, where the WRF estimates almost overlap the observational curve. However, these configurations substantially overestimate precipitation in certain months over the north and east regions.

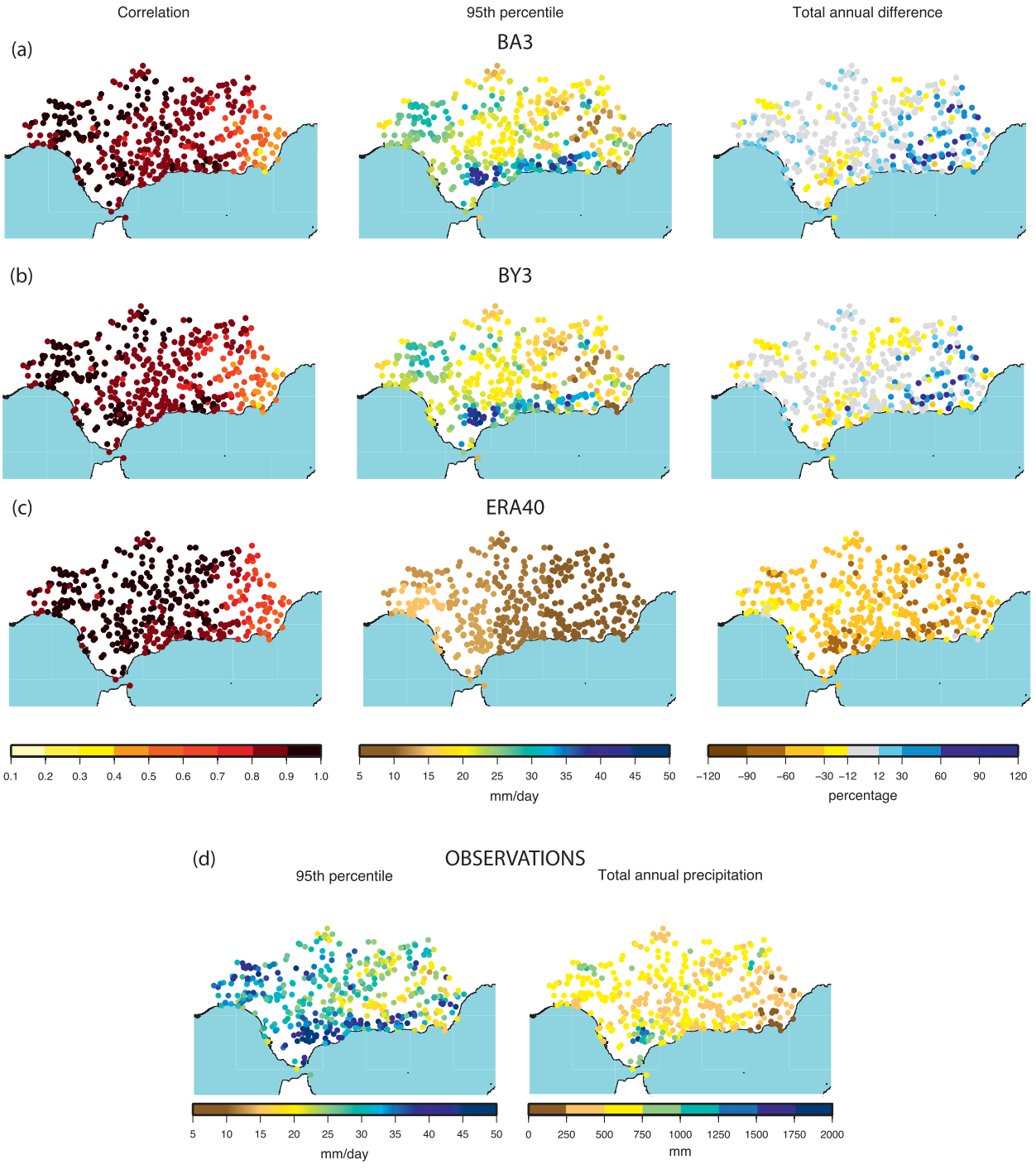

FIG. 6. (left to right) Spatial distribution of monthly precipitation correlation coefficient, 95th daily precipitation percentile, and difference with respect to observed total annual precipitation calculated station by station for (a) BA3, (b) BY3, and (c) ERA-40. (d) Observed 95th daily precipitation percentile and total annual rainfall.

3) SPATIAL DISTRIBUTION OF PRECIPITATION

Besides WRF evaluation using regionalization, validation was also performed station by station. Figure 6 shows the spatial distribution of the correlation coefficient of monthly precipitation, the mean annual difference of rainfall, and the 95th percentile for the BA3 and BY3 configurations, as well as the ERA-40 data and the observations. By means of this analysis, orographic impacts can be explored along with mesoscale dynamics and

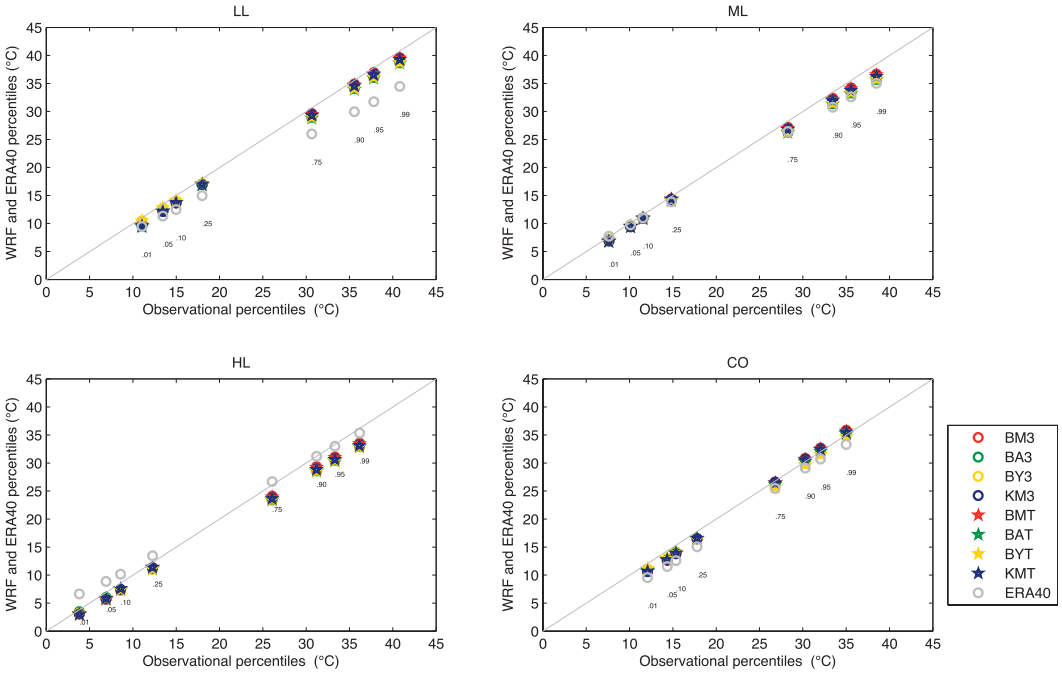

FIG. 7. Daily maximum temperature percentiles simulated by various WRF configurations and ERA-40 vs observational percentiles for the different temperature regions. Gray line indicates a perfect description of the PDF.

descriptions of local climate features. Rather than the WRF capabilities at individual station, which might be affected by the representation error, the aim of this comparison was to depict the spatial patterns of the model accuracy.

Correlations show an evident zonal gradient with higher values in the western part (0.90–1.00) decreasing to the east with values of 0.30–0.40 at certain stations. Annual differences in precipitation give an idea of the areas where rainfall is generally over- or underestimated, and it is important to note that most of the stations in the Guadalquivir River basin (the west and central regions) present deviations lower than 10%. In addition, it can be observed that precipitation is shifted eastward as a consequence of unresolved topography. A negative difference is thus located in the western part because topography was smoothed and precipitation not induced, while a positive deviation was found in the easternmost areas, where the highest mountains force the precipitation that did not fall upwind.

The spatial distribution of the 95th percentile for daily precipitation is clearly an improvement over ERA-40 (Fig. 6), which only resolves a broad gradient toward lower values in the east. In fact, WRF is largely able to capture topographic effects on extremes, particularly over mountainous regions (Sierra de Grazalema and Sierra Nevada, in the south), although their intensity is slightly diminished. This feature strongly emphasizes the convenience and benefit of using RCMs, primarily in terms of precipitation extremes, which is one of the main aspects to be surveyed in climate change studies.

b. *Temperature results*

Surface temperatures in WRF were compared at every time step and maximum and minimum values were stored on a daily basis. To refer grid-points and observations to common altitudes, the WRF outputs were adjusted using a standard environmental lapse rate (6.5 K km^{-1}) to account differences in elevation between the observations and the nearest grid-points. Observations and WRF results were then compared using the multistep methodology, described in section 3b, to group them into regions.

1) DAILY VALUES OF MAXIMUM AND MINIMUM TEMPERATURES

All daily values from each region were considered to calculate eight percentiles (1st, 5th, 10th, 25th, 75th, 90th, 95th, and 99th) for both T_{max} and T_{min}. Figures 7 and 8 show percentiles from different WRF runs versus observational percentiles for T_{max} and T_{min}, respectively, with the gray line representing a perfect description of the PDF. Percentiles from ERA-40 temperatures are shown too.

Minor differences were observed among the explored configurations, since temperatures in RCMs mostly

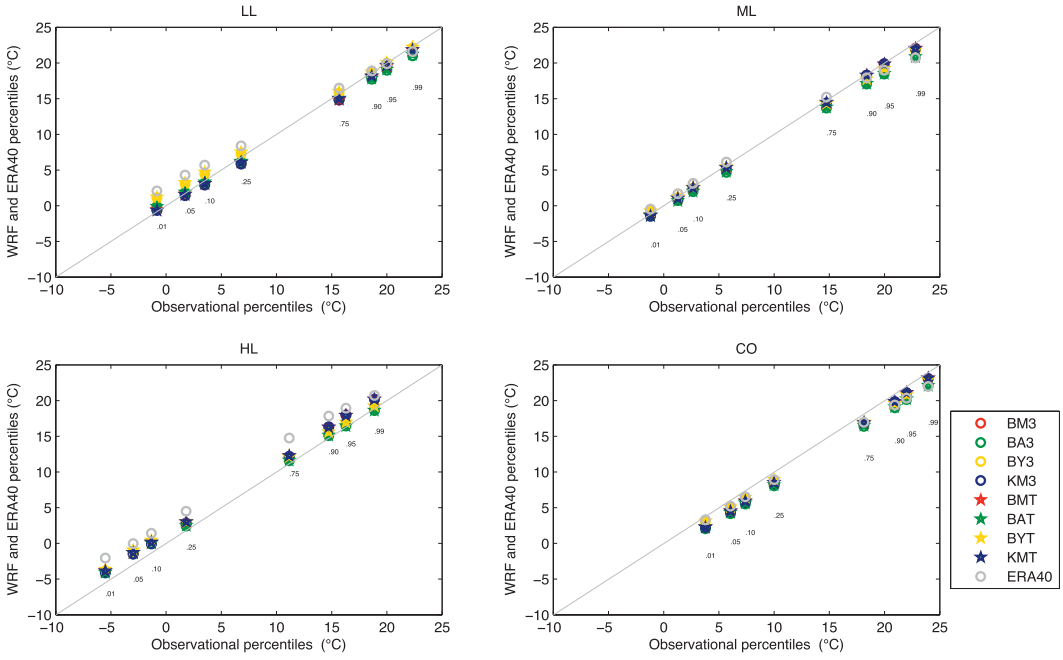

FIG. 8. As in Fig. 7, but for daily T_{min}.

depend on model elevation, radiation schemes, and SST. Although these are minor differences, it is important to analyze WRF performance in terms of temperature as well.

Both T_{max} and T_{min} percentiles are accurately captured by WRF, with slightly better results for the latter. Estimations of maximum temperature show a minor underestimation, except for the CO region, where no clear tendency was observed. In fact, in the CO region, WRF tends to produce higher summer temperature extremes (large percentiles) probably due to an intensification of the land influence to the detriment of the sea influence. The spread of WRF estimates in minimum temperature is somewhat wider (lower percentiles in the LL and upper percentiles in the HL); however, the differences in percentiles are still not noteworthy.

In comparison with ERA-40, two important aspects are improved when applying dynamical downscaling. First, higher extremes of maximum temperatures are much better reproduced in the LL region, where the surface temperature extremes attain the highest values in all of Europe. Second, minimum percentiles are captured more accurately in the HL region, which basically represents locations at high altitudes and thus where the absolute temperature minima are reached in Andalusia. In contrast, maximum temperature percentiles in the HL are well described by ERA-40, whereas WRF seems to produce colder extremes. In the ML and CO regions, only slight improvements are achieved with WRF.

2) MONTHLY VALUES OF MAXIMUM AND MINIMUM TEMPERATURES

Mean values of daily T_{max} and T_{min} were calculated for every station and its associated WRF grid point, and then averaged over the regions to compare them. Figures 9 and 10 show the correlation coefficient, the RMSE, and the MAE between WRF and observations' monthly means for both T_{max} and T_{min}. ERA-40 monthly means are shown as well.

Although correlation coefficient values are almost indistinguishable for WRF and ERA-40 estimates—within the bounds of 0.98–0.99 for T_{max} and 0.97–0.99 for T_{min}—both RMSE and MAE show sharp distinctions even among the WRF simulations. In regions LL and CO, the reduction of errors for WRF data is significant with respect to ERA-40 for T_{max} and likewise in regions LL, H, and CO for T_{min}. In fact, RMSE is improved from about 4° to about 2°C and a similar contribution of WRF was observed for MAE in the LL region. In the case of minimum temperature, it is the HL region that is most sensitive to the model, decreasing RMSE from about 3° to about 2°C. In every region most WRF results outperform ERA-40 in terms of monthly means of T_{max} and T_{min}.

As for the performance of individual WRF configurations, the combination BMJ–YSU appears to be the most appropriate to describe monthly-mean minimum temperature, whereas BMJ–MYJ seems to better

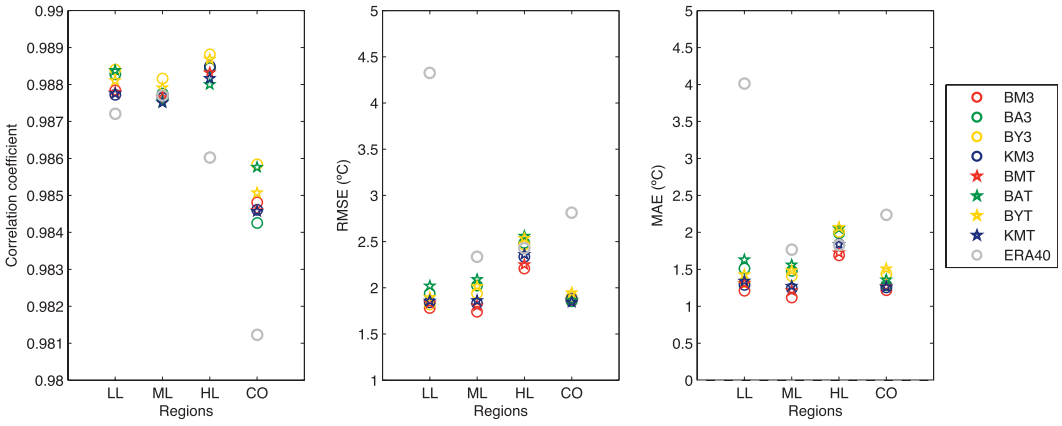

FIG. 9. (left to right) Correlation coefficient, RMSE, and MAE calculated for WRF and ERA-40 monthly-mean T_{max} with respect to observations in the different temperature regions.

reproduce monthly-mean maximum temperature. It should be noted that PBL parameterization plays a significant role in describing surface variables, particularly at night, and thus it is the scheme with the highest impact on temperature, especially on the minimum values. In fact, configurations that include the same PBL scheme usually perform very similarly (KF–MYJ and BMJ–MYJ) as can be seen in Fig. 10. Conversely, the choice of microphysics has negligible repercussions on temperature estimations as has occurred for precipitation, and indeed similar conclusions have been drawn in previous studies over the Iberian Peninsula (Fernández et al. 2007).

The annual cycle was also calculated and it is displayed in Fig. 11. Its shape is precisely captured although some deviations were found in certain seasons. Maximum temperature is, in general, underestimated, specifically during the summer, apart from the CO region. For the rest of the regions, WRF compares much better with observations, apart from March for LL, July for ML, and January for CO. In contrast, there is no clear propensity in the sign of the minimum temperature deviations, excluding CO, where every WRF configuration presents a cold bias. Likewise, in compliance with how similarly WRF configurations reproduce the annual cycle, no conclusion can be drawn in relation to the most suitable physics combination.

Considering the ERA-40 annual cycles for both temperatures extremes, WRF contributes to improve the temperature description in a few situations (T_{max} in LL and CO, and T_{min} in HL and LL). Nevertheless, the annual cycle is reproduced similarly by ERA-40 and WRF in the other situations.

3) SPATIAL DISTRIBUTION OF MAXIMUM AND MINIMUM TEMPERATURES

The correlation coefficient and the bias of monthly values, together with the 95th percentile for T_{max} and 5th for T_{min} were calculated station by station for every WRF simulation. To illustrate the spatial distribution of these parameters in southern Spain, results from

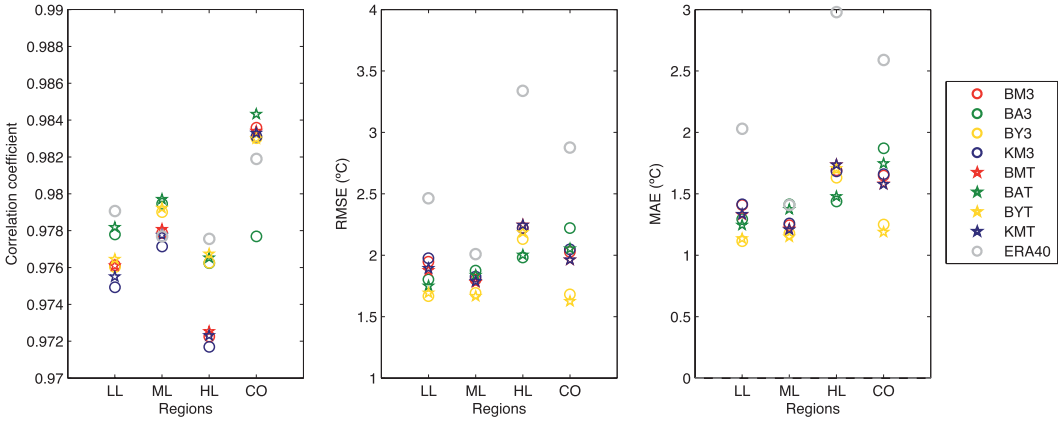

FIG. 10. As in Fig. 9, but for monthly-mean T_{min}.

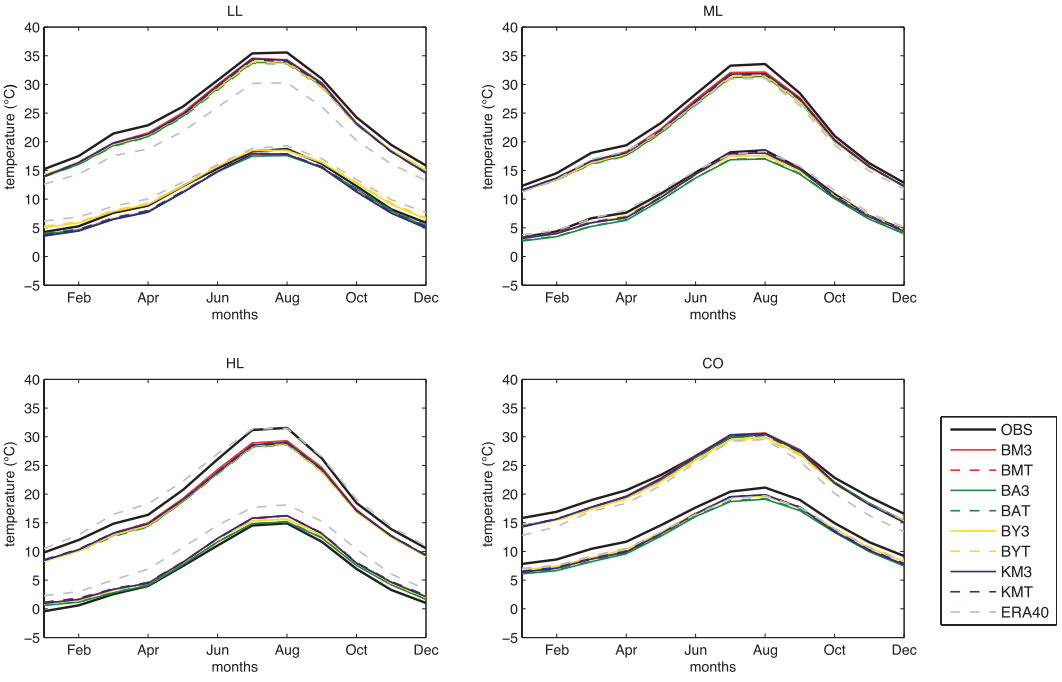

FIG. 11. Annual cycle for T_{max} and T_{min} for the different temperature regions: observations (black), ERA-40 (gray dashed), and WRF simulations (colors).

simulations BA3 and BY3 are shown in Fig. 12 (T_{max}) and Fig. 13 (T_{min}). The same parameters were also calculated for ERA-40 to evidence the improvements from dynamical downscaling. The observed extreme percentiles, along with the mean throughout the entire period, are shown too as a means to set a frame of reference.

The temperature correlation spatial patterns are not as definite as for precipitation; however, T_{max} interannual variability is better captured in the Guadalquivir River basin and higher values can be observed in this area. The quantity T_{min} presents lower correlation coefficient values over the entire region, a feature that is related to PBL parameterization and was also found by Zhang et al. (2009) in the U.S. Pacific Northwest. At most stations, WRF T_{min} is correlated over 0.95 with observations, although very few stations show values below that threshold and are thus off the scale, particularly for BA3 and ERA-40. Nonetheless, excluding Marbella (0.75), these stations still present high correlations exceeding 0.90.

Although both WRF configurations tend to capture adequately the maxima over the river basin, some deficiencies were noted. The regional model provides values that are too low over the eastern mountains, particularly the BA3 combination whose differences versus observations are about 4°C at many mountain stations, whereas these differences range between 0° and 1°C in the Guadalquivir River basin. The northeastern mountains are also problematic with regard to T_{min} extremes, with marked overestimations produced by both WRF configurations. Nevertheless, WRF minimum temperature percentiles show fair agreement with observations in general. In fact, at more than 70% of the stations, 5th percentile WRF and observation differences are in the −2° to 2°C range. The main distinction between the WRF simulations was found in the river basin, where BY3 produces warmer minima toward the interior.

As would be expected from its coarse resolution, ERA-40 scarcely captures the spatial pattern of extremes, while WRF clearly improves their distribution and magnitude thanks to the finer resolution. Compared to ERA-40, WRF better reproduces the maximum extremes in the lower elevations and minimum values over the mountains, as well as milder T_{min} at the coast and lower T_{max} at high altitudes.

In accordance with the results from the annual cycle, T_{max} is broadly underestimated over the entire region, whereas no clear tendency was observed for T_{min}. These results are shown for both WRF configurations in Figs. 12 and 13 and they yield similar values in terms of monthly temperatures. Only minor differences can be noted in the case of T_{min}, with BA3 being colder than BY3. ERA-40 biases with respect to observations are remarkable, particularly over the river basin for T_{max} and the west for T_{min}.

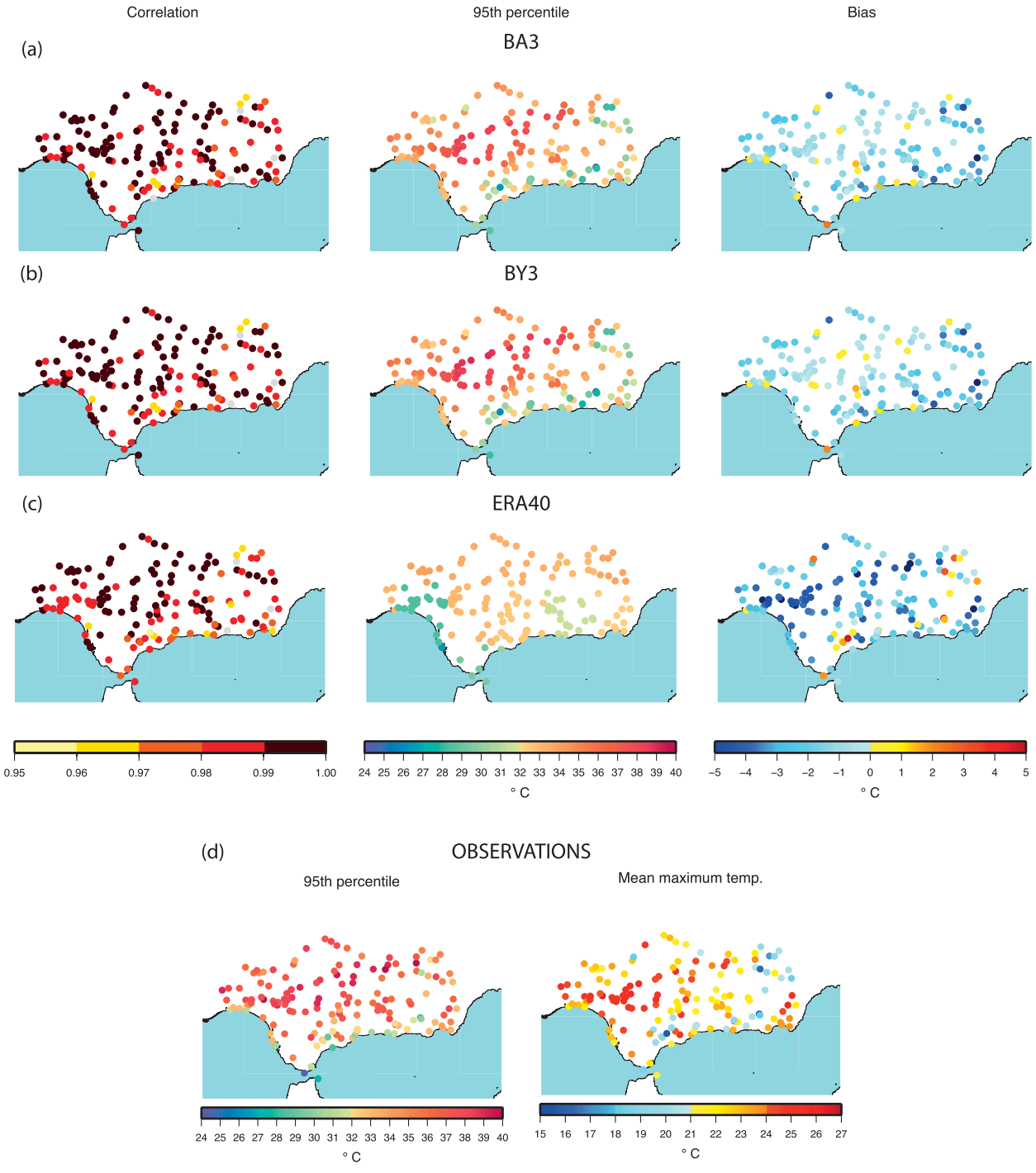

FIG. 12. (left to right) Spatial distribution of monthly-mean T_{max} correlation coefficient, 95th daily T_{max} percentile, and the bias with respect to observations: (a) BA3, (b) BY3, and (c) ERA-40. Gray dots represent values below the scale bounds. (d) Observed 95th daily T_{max} percentile and mean T_{max}.

5. Summary and conclusions

The WRF model has been shown to improve temperature and precipitation predictions in terms of frequency, spatial distribution, and intensity of extreme events with respect to ERA-40 data over the complex terrain region of Andalusia. Not only resolution but also physics parameterizations have a significant impact on results, as observed in the spread of the different configuration estimates.

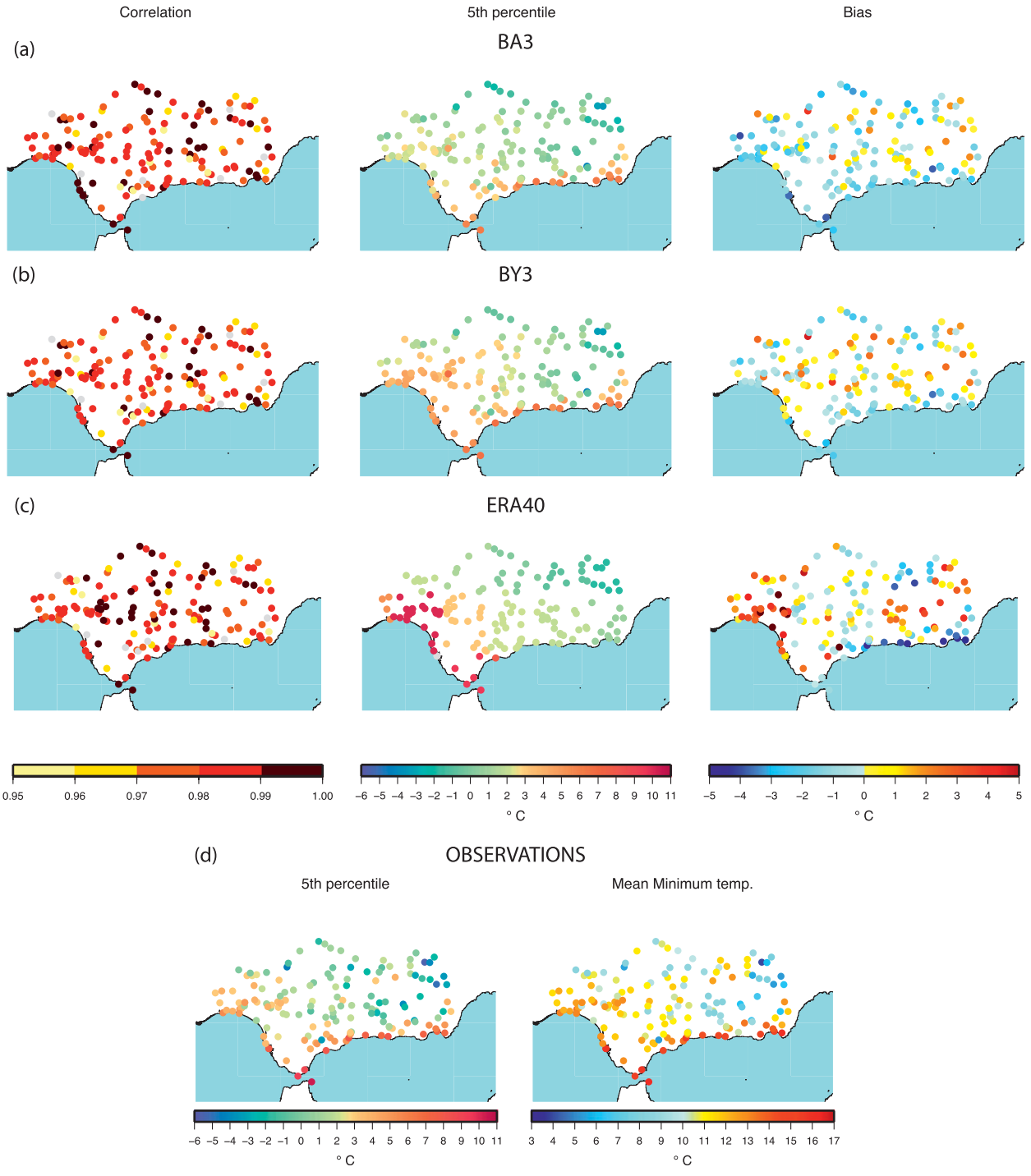

FIG. 13. As in Fig. 11, but for daily T_{min} and using the 5th percentile.

Most parameters explored were noticeably improved by WRF, except for the monthly correlation that presented similar or lower values than ERA-40. However, these imperfections are not crucial from a climatic perspective. Precipitation was particularly improved by WRF in terms of biases and relative RMSE, whereas minor differences were found for both T_{max} and T_{min}. Spatial distributions were markedly enhanced by WRF, providing value-added details of local heavy rainfall events or temperature elevation dependence.

The question of which WRF configuration outperforms the others in every variable and in any situation

remains unanswered, since it strongly depends on the region and the season considered. Although the complete spectrum of physics options has not been examined, the analysis carried out sheds light on the suitability of certain configurations. For instance, cumulus and PBL schemes have been revealed as chief components in the description of precipitation in southern Spain, whereas the microphysics choice seemed to be of minor importance. Overall, the combinations BMJ–ACM2 and BMJ–YSU compared best with observations. The simplest microphysics scheme tested was recommended (WSM3). Regarding temperature, almost no differences could be appreciated among the varying configurations, and only the PBL scheme affects $T_{\min}$ because it is directly related to the nocturnal boundary layer simulation. The MYJ scheme provided slightly better results. Temperature variations were rather smooth in both time and space, as well as highly subject to elevations. These two factors imply that the explored physics parameterizations have less effect on temperature than on precipitation. Bearing in mind that major differences in WRF estimates were found with respect to rainfall, the configurations suggested for precipitation prevail over those for temperature.

The main conclusion that can be drawn from this study is that WRF accurately reproduces Andalusian climate features at several time scales. Additionally, it provides information at spatial scales not resolved by GCMs that can be extremely useful in the elaboration of high-resolution climate change scenarios. Further research must be carried out to extend these conclusions to climate reference periods.

Acknowledgments. The Spanish Ministry of Science and Innovation with additional support from the European Community funds (FEDER), Project CGL2007-61151/CLI, and the Regional Government of Andalusia, Project P06-RNM-01622, have financed this study. The Centro de Servicios de Informática y Redes the Comunicaciones (CSIRC), Universidad de Granada, has provided the computing time. We thank the National Center for Atmospheric Research (NCAR), Boulder, Colorado, for its direct collaboration in this paper. ERA-40 data were obtained from ECWMF. We thank Dr. Andrew S. Kowalski for his comments and suggestions, which enhanced the clarity of this work. We also thank three reviewers for their valuable comments, which improved the final version of this manuscript.

REFERENCES

Amengual, A., R. Romero, V. Homar, C. Ramis, and S. Alonso, 2007: Impact of the lateral boundary conditions resolution on dynamical downscaling of precipitation in mediterranean Spain. *Climate Dyn.,* **29,** 487–499.

Bärring, L., 1987: Spatial patterns of daily rainfall in central Kenya–Application of principal component analysis, common factor analysis and spatial correlation. *Int. J. Climatol.,* **7,** 267–289.

Bell, J., L. Sloan, and M. Snyder, 2004: Regional changes in extreme climatic events: A future climate scenario. *J. Climate,* **17,** 81–87.

Borge, R., V. Alexandrov, J. José del Vas, J. Lumbreras, and E. Rodríguez, 2008: A comprehensive sensitivity analysis of the WRF model for air quality applications over the Iberian Peninsula. *Atmos. Environ.,* **42,** 8560–8574.

Bukovsky, M. S., and D. J. Karoly, 2009: Precipitation simulations using WRF as a nested regional climate model. *J. Appl. Meteor. Climatol.,* **48,** 2152–2159.

Bunkers, M., J. Miller, and A. DeGaetano, 1996: Definition of climate regions in the northern plains using an objective cluster modification technique. *J. Climate,* **9,** 130–146.

Caldwell, P., H.-N. S. Chin, D. C. Bader, and G. Bala, 2009: Evaluation of a WRF dynamical downscaling simulation over California. *Climatic Change,* **95,** 499–521.

Calinski, R. B., and J. Harabasz, 1974: A dendrite method for cluster analysis. *Commun. Stat.,* **3,** 1–27.

Catalano, F., and A. Cenedese, 2010: High-resolution numerical modeling of thermally driven slope winds in a valley with strong capping. *J. Appl. Meteor. Climatol.,* **49,** 1859–1880.

——, and C.-H. Moeng, 2010: Large-eddy simulation of the daytime boundary layer in an idealized valley using the Weather Research and Forecasting numerical model. *Bound.-Layer Meteor.,* **137,** 49–75.

Christensen, O., M. Gaertner, J. Prego, and J. Polcher, 2001: Internal variability of regional climate models. *Climate Dyn.,* **17,** 875–887.

Deb, S., T. Srivastava, and C. Kishtawal, 2008: The WRF model performance for the simulation of heavy precipitating events over Ahmedabad during August 2006. *J. Earth Syst. Sci.,* **117,** 589–602.

Denis, B., R. Laprise, and D. Caya, 2003: Sensitivity of a regional climate model to the resolution of the lateral boundary conditions. *Climate Dyn.,* **20,** 107–126.

Dickinson, R., R. Errico, F. Giorgi, and G. Bates, 1989: A regional climate model for the western United States. *Climatic Change,* **15,** 383–422.

Evans, J. P., and M. F. McCabe, 2010: Regional climate simulation over Australia's Murray-Darling Basin: A multitemporal assessment. *J. Geophys. Res.,* **115,** D14114, doi:10.1029/2010JD013816.

Fernández, J., 2004: Statistical and dynamical downscaling models applied to winter precipitation on the Cantabrian coast. Ph.D. thesis, University of the Basque Country, 124 pp.

——, J. P. Montávez, J. Sáenz, J. F. González-Rouco, and E. Zorita, 2007: Sensitivity of the MM5 mesoscale model to physical parameterizations for regional climate studies: Annual cycle. *J. Geophys. Res.,* **112,** D04101, doi:10.1029/2005JD006649.

Fita, L., J. Fernández, and M. García-Díez, 2010: CLWRF: WRF modifications for regional climate simulation under future scenarios. Preprints, *11th WRF Users' Event,* Boulder, CO, NCAR, P-26.

Fovell, R., 1997: Consensus clustering of U.S. temperature and precipitation data. *J. Climate,* **10,** 1405–1427.

——, and M. Fovell, 1993: Climate zones of the conterminous United States defined using cluster analysis. *J. Climate,* **6,** 2103–2135.

Frei, C., J. H. Christensen, M. Déqué, D. Jacob, R. G. Jones, and P. L. Vidale, 2003: Daily precipitation statistics in regional climate models: Evaluation and intercomparison for the European Alps. *J. Geophys. Res.,* **108,** 4124, doi:10.1029/2002JD002287.

Gallus, W., Jr., and J. Bresch, 2006: Comparison of impacts of WRF dynamic core, physics package, and initial conditions on warm season rainfall forecasts. *Mon. Wea. Rev.,* **134,** 2632–2641.

Gerstengarbe, F.-W., P. C. Werner, and K. Fraedrich, 1999: Applying non-hierarchical cluster analysis algorithms to climate classification: Some problems and their solution. *Theor. Appl. Climatol.,* **64,** 143–150.

Gillett, N., and D. Thompson, 2003: Simulation of recent Southern Hemisphere climate change. *Science,* **302,** 273.

Giorgi, F., 2006: Regional climate modeling: Status and perspectives. *J. Phys. IV,* **139,** 101–118.

——, and L. Mearns, 1999: Introduction to special section: Regional climate modeling revisited. *J. Geophys. Res.,* **104,** 6335–6352.

Göber, M., E. Zsótér, and D. Richardson, 2008: Could a perfect model ever satisfy a naïve forecaster? On grid box mean *versus* point verification. *Meteor. Appl.,* **15,** 359–365.

Gong, X., and M. Richman, 1995: On the application of cluster analysis to growing season precipitation data in North America east of the Rockies. *J. Climate,* **8,** 897–931.

Herrera, S., L. Fita, J. Fernández, and J. M. Gutiérrez, 2010: Evaluation of the mean and extreme precipitation regimes from the ENSEMBLES regional climate multimodel simulations over Spain. *J. Geophys. Res.,* **115,** D21117, doi:10.1029/2010JD013936.

Hong, S. Y., K. S. S. Lim, J. H. Kim, J. O. J. Lim, and J. Dudhia, 2009: Sensitivity study of cloud-resolving convective simulations with WRF using two bulk microphysical parameterizations: Ice-phase microphysics versus sedimentation effects. *J. Appl. Meteor. Climatol.,* **48,** 61–76.

Jankov, I., W. Gallus Jr., M. Segal, B. Shaw, and S. Koch, 2005: The impact of different WRF model physical parameterizations and their interactions on warm season MCS rainfall. *Wea. Forecasting,* **20,** 1048–1060.

Jiménez, P., E. García-Bustamante, J. F. González-Rouco, F. Valero, J. Montávez, and J. Navarro, 2008: Surface wind regionalization in complex terrain. *J. Appl. Meteor. Climatol.,* **47,** 308–325.

Kain, J. S., S. J. Weiss, J. J. Levit, M. E. Baldwin, and D. R. Bright, 2006: Examination of convection-allowing configurations of the WRF model for the prediction of severe convective weather: The SPC/NSSL spring program 2004. *Wea. Forecasting,* **21,** 167–181.

Kalkstein, L., G. Tan, and J. Skindlov, 1987: An evaluation of three clustering procedures for use in synoptic climatological classification. *J. Climate Appl. Meteor.,* **26,** 717–730.

Köppen, W., 1923: *Die Klimate der Erde, Grundriss der Klimakunde*. De Greyter, 369 pp.

Kostopoulou, E., K. Tolika, I. Tegoulias, C. Giannakopoulos, S. Somot, C. Anagnostopoulou, and P. Maheras, 2009: Evaluation of a regional climate model using in situ temperature observations over the Balkan Peninsula. *Tellus,* **61A,** 357–370.

Kwun, J. H., Y. K. Kim, J. W. Seo, J. H. Jeong, and S. H. You, 2009: Sensitivity of MM5 and WRF mesoscale model predictions of surface winds in a typhoon to planetary boundary layer parameterizations. *Nat. Hazards,* **51,** 63–77.

Laprise, R., 2008: Regional climate modelling. *J. Comput. Phys.,* **227,** 3641–3666.

——, and Coauthors, 2008: Challenging some tenets of regional climate modelling. *Meteor. Atmos. Phys.,* **100,** 3–22.

Leung, L. R., L. O. Mearns, F. Giorgi, and R. L. Wilby, 2003: Regional climate research: Needs and opportunities. *Bull. Amer. Meteor. Soc.,* **84,** 89–95.

Li, X., and Z. Pu, 2009: Sensitivity of numerical simulations of the early rapid intensification of Hurricane Emily to cumulus parameterization schemes in different model horizontal resolutions. *J. Meteor. Soc. Japan,* **87,** 403–421.

Lund, R., and B. Li, 2009: Revisiting climate region definitions via clustering. *J. Climate,* **22,** 1787–1800.

McGregor, J., 1997: Regional climate modelling. *Meteor. Atmos. Phys.,* **63,** 105–117.

Miguez-Macho, G., G. L. Stenchikov, and A. Robock, 2004: Spectral nudging to eliminate the effects of domain position and geometry in regional climate model simulations. *J. Geophys. Res.,* **109,** D13104, doi:10.1029/2003JD004495.

Milligan, G., 1980: An examination of the effect of six types of error perturbation on fifteen clustering algorithms. *Psychometrika,* **45,** 325–342.

Mitchell, T. D., T. R. Carter, P. D. Jones, M. Hulme, and M. New, 2004: A comprehensive set of high-resolution grids of monthly climate for Europe and the globe: The observed record (1901-2000) and 16 scenarios (2001-2100). Tyndall Centre Working Paper 55, 25 pp.

Moberg, A., and P. Jones, 2004: Regional climate model simulations of daily maximum and minimum near-surface temperatures across Europe compared with observed station data 1961–1990. *Climate Dyn.,* **23,** 695–715.

Nolan, D. S., J. A. Zhang, and D. P. Stern, 2009: Evaluation of planetary boundary layer parameterizations in tropical cyclones by comparison of in situ observations and high-resolution simulations of Hurricane Isabel (2003). Part I: Initialization, maximum winds, and the outer-core boundary layer. *Mon. Wea. Rev.,* **137,** 3651–3674.

North, G., T. Bell, R. Cahalan, and F. Moeng, 1982: Sampling errors in the estimation of empirical orthogonal functions. *Mon. Wea. Rev.,* **110,** 699–706.

Osborn, T., 2004: Simulating the winter North Atlantic Oscillation: The roles of internal variability and greenhouse gas forcing. *Climate Dyn.,* **22,** 605–623.

Preisendorfer, R. W., 1988: *Principal Component Analysis in Meteorology and Oceanography*. Elsevier, 425 pp.

Radu, R., M. Déqué, and S. Somot, 2008: Spectral nudging in a spectral regional climate model. *Tellus,* **60A,** 898–910.

Reid, S., and R. Turner, 2001: Correlation of real and model wind speeds in different terrains. *Wea. Forecasting,* **16,** 620–627.

Richman, M., and P. Lamb, 1985: Climatic pattern analysis of three- and seven-day summer rainfall in the central United States: Some methodological considerations and a regionalization. *J. Climate Appl. Meteor.,* **24,** 1325–1343.

Rivington, M., D. Miller, K. Matthews, G. Russell, G. Bellocchi, and K. Buchan, 2007: Downscaling regional climate model estimates of daily precipitation, temperature and solar radiation data. *Climate Res.,* **35,** 181.

——, ——, ——, ——, ——, and ——, 2008: Evaluating regional climate model estimates against site-specific observed data in the UK. *Climatic Change,* **88,** 157–185.

Romero, R., C. Ramis, J. Guijarro, and G. Sumner, 1999: Daily rainfall affinity areas in mediterranean Spain. *Int. J. Climatol.,* **19,** 557–578.

Sertel, E., A. Robock, and C. Ormeci, 2009: Impacts of land cover data quality on regional climate simulations. *Int. J. Climatol.,* **30,** 1942–1953.

Seth, A., and F. Giorgi, 1998: The effects of domain choice on summer precipitation simulation and sensitivity in a regional climate model. *J. Climate,* **11,** 2698–2712.

Skamarock, W. C., and Coauthors, 2008: A description of the Advanced Research WRF version 3. NCAR Tech. Note NCAR/TN-475+STR, 125 pp. [Available online at http://www.mmm.ucar.edu/wrf/users/docs/arw_v3.pdf.]

Solomon, S., D. Qin, M. Manning, M. Marquis, K. Averyt, M. M. B. Tignor, H. L. Miller Jr., and Z. Chen, Eds., 2007: *Climate Change 2007: The Physical Science Basis*. Cambridge University Press, 996 pp.

Thornthwaite, C., 1931: The climates of North America: According to a new classification. *Geogr. Rev.,* **21,** 633–655.

Unal, Y., T. Kindap, and M. Karaca, 2003: Redefining the climate zones of Turkey using cluster analysis. *Int. J. Climatol.,* **23,** 1045–1055.

Zhang, Y., V. Duliere, P. W. Mote, and E. P. Salathe, 2009: Evaluation of WRF and HadRM mesoscale climate simulations over the U.S. Pacific Northwest. *J. Climate,* **22,** 5511–5526.